RESEARCH ON ELECTRICAL DISCHARGE MACHINING (EDM) ROUGHENING PROCESS BASED ON SURFACE ELECTROMAGNETIC SHIELDING PERFORMANCE

Dong CAI[1]*, Wenming DENG[2], Qianxing HUANG[3]

According to the absorption mechanism of surface morphology in electric discharge machining, the absorption characteristics of different surface morphologies are different, that is, the electromagnetic shielding effect is different. The main factor affecting the morphology characteristics of the surface is the processing of electrical parameters. To seek the electromagnetic shielding effect of roughened surfaces under different electrical parameter processing conditions, this study conducted process experiments and simulation experiments on non-magnetic steel surfaces using electric discharge machining and studied the influence of peak current and pulse width on the electromagnetic shielding effect of roughened surfaces. The research results suggest that the absorption rate of the roughened surface decreases with increasing pulse width, with the increase of peak current, there is a tendency of initial decrease followed by a subsequent increase. In addition, the absorption rate of the roughened surface shows an overall increasing trend with the ratio of surface pit depth to diameter. Therefore, providing effective reference for improving the electromagnetic shielding performance of material surfaces.

Keywords: electric spark, peak current, pulse width, surface topography, absorption rate

1. Introduction

Presenting concave and convex structures under electron microscopy, surface morphology of the traction converter box of high-speed train after rough machining by electric discharge machine tool, this surface microstructure can to some extent prevent electromagnetic interference between the electrical equipment inside the high-speed train and the outside world during high-speed operation, has certain electromagnetic shielding characteristics. Currently, Wu et al. [1] have studied the machining efficiency and surface quality of workpieces using electrical discharge machining (EDM) methods. Padhy et al. [2] have used brass wire as the

[1]* Lecturer, College of Railway Locomotive and Rolling Stock, Liuzhou Railway Vocational and Technical College, email: 1756379127@qq.com (corresponding author)
[2] Lecturer, College of Railway Locomotive and Rolling Stock, Liuzhou Railway Vocational and Technical College, email: 565544053@qq.com
[3] Lecturer, College of Railway Locomotive and Rolling Stock, Liuzhou Railway Vocational and Technical College, email: hqxwhh@163.com

tool electrode and conducted orthogonal experiments to investigate the influence of electrical parameters on discharge channels. Sun et al. [3] conducted electrical discharge machining experiments on Zr-4 alloy to study its microstructure, and found that the surface of the alloy after electrical discharge machining has been improved in terms of mechanical properties, smoothness, and corrosion resistance. Sedat et al. [4] studies the optimal machining conditions for surface roughness and material removal rate by controlling parameters such as pulse current, pulse duration, and off time in electrical discharge machining. Iqbal et al. [5] used metal carbides as electromagnetic shielding materials and experimentally studied the electromagnetic wave interaction principle under the MXenes electromagnetic interference shielding mechanism. Yang et al. [6] proposed an interference suppression method for electromagnetic shielding through simulation estimation and experimental verification under the system common mode interference calculation model. Zhang and Wang [7] proposed using a method of metalized carbon fiber interlayer to enhance the electromagnetic protection performance of the traction inverter box. Devika et al. [8] concluded through dielectric property testing and analysis of polydimethylsiloxane composite materials that composites doped with dimethylsiloxane exhibit superior shielding efficiency. In the relevant research fields at home and abroad, however, there is a relative lack of exploration and practice in applying the technique of surface morphology roughening to electromagnetic shielding scenarios. The related public research results and systematic analysis are still relatively scarce. Therefore, studying the influence of surface morphology roughening by electric discharge on electromagnetic shielding effect has strong feasibility and innovation.

To study the influence characteristics of electrical parameters on the surface morphology of roughened surfaces and the electromagnetic shielding effect, an experimental study was conducted using peak current, pulse width, and pulse interval as control variables in electrical parameter control. Among them, the peak current size characterizes the plasma density in the discharge channel during the electric discharge machining process. The pulse width size characterizes the duration of a single processing operation. Electric discharge machining (EDM) represents a continuous discharge process formed by the accumulation of a single electrical discharge (single pulse discharge), and the pulse interval only characterizes the duration of the single discharge interval in EDM during continuous discharge (multi pulse discharge) machining [9,10], research has shown that peak current and pulse width affect the energy level of electrical machining, while pulse interval does not change the energy level during the machining process of the workpiece. Therefore, pulse interval does not affect the surface morphology of the roughened surface [11]. Therefore, this paper selects two major electrical parameters, peak current and pulse width, and adopts a two factor six level orthogonal experimental scheme. Through extensive experimental research and simulation analysis, the relationship between electrical parameters and the electromagnetic shielding effect of frosted surfaces is sought, which provides reference value for improving the electromagnetic shielding performance of traction inverter boxes.

2. Electric spark fuzz experiment

The experiment used non-magnetic steel as the workpiece material and employed Hitachi Mitsubishi EA12D CNC EDM machine for rough machining. Stable kerosene was used as the working fluid [12-14]. The electrode material selected is graphite, which has excellent mechanical processing performance, low thermal expansion, and high melting point, as the tool electrode [15,16]. The electrical parameters mainly include two variables: peak current and pulse width. Peak current is indicative of the energy per single pulse discharge, while pulse interval only represents the time interval of per single pulse discharge during a continuous multi pulse discharge process [17]. After research and analysis, it was found that pulses do not affect the surface morphology characteristics of roughened surfaces. Therefore, in this study, pulse width Ton and peak current Ip were used as the main control parameters for grouped experiments. Considering the scientific and feasible nature of experimental data acquisition, a two factor six level orthogonal experiment was adopted in this experimental study, and the orthogonal experimental table is shown in Table 1.

Table 1

Orthogonal test table

peak current I_p (A)	**pulse width T_{on} (μs)**
10, 23, 35	5.2, 7.6, 9.6
47, 60, 75	11.2, 13.6, 15.2

The surface of non-magnetic steel treated with electric spark texturing presents dense and irregular surface features such as granular, spherical, cracked, and surface melted shapes. Through theoretical and extensive experimental research, as well as simulation analysis, it is known that this dense concave convex surface structure has certain absorption characteristics. Therefore, when applied in the structure of the traction inverter box of high-speed trains, it can maximize electromagnetic shielding without changing the structure of the traction inverter. To investigate the specific properties and laws of the surface morphology of non-magnetic steel under different electrical parameter processing conditions, and to provide reference for the subsequent surface texturing of the traction inverter box, several groups of non-magnetic steels with typical morphological characteristics were selected for the experiment, and the surface microstructural morphologies observed under scanning electron microscope of field emission were obtained. The roughened samples treated by electric discharge machining machine are shown in Figure 1 and scanning electron microscope of field emission are shown in Figure 2.

Fig. 1 Electric Spark Texturing Sample

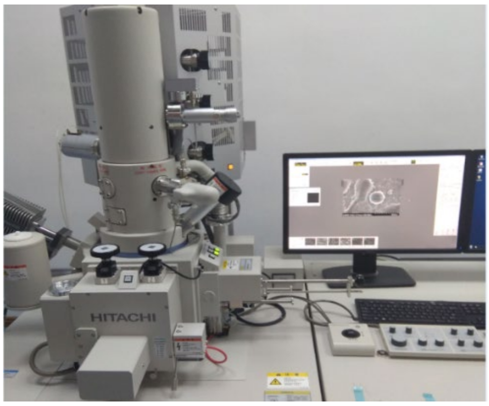

Fig. 2 SEM of field emission

3. Analysis of Fuzzy Surface Morphology Characteristics

(1) Microcracks. The electrical parameters were as follows: (a) Ip=23 A, Ton=5.2 μs, (b) Ip=47 A, Ton=5.2 μs, (c) Ip=23 A, Ton=15.2 μs, (d) Ip=47 A, Ton=15.2 μs. The special morphologies of the microstructure on the textured surface after electrical discharge machining were identified under scanning electron microscope of field emission, as is evident in Figure 3.

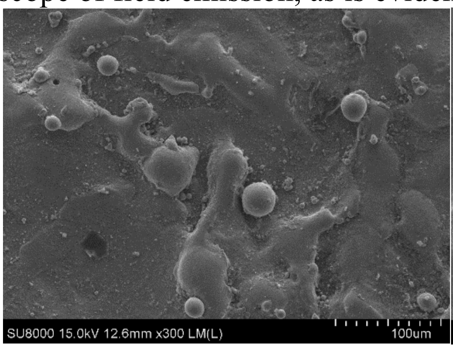

(a)Ip=23 A and Ton=5.2μs

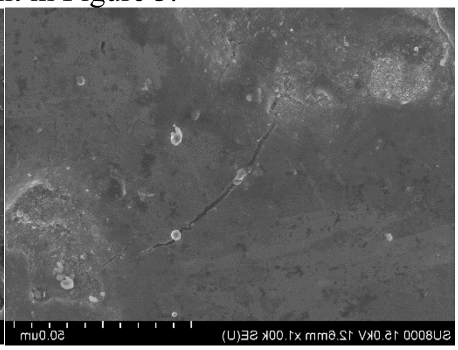

(b) Ip=47 A and Ton=5.2μs

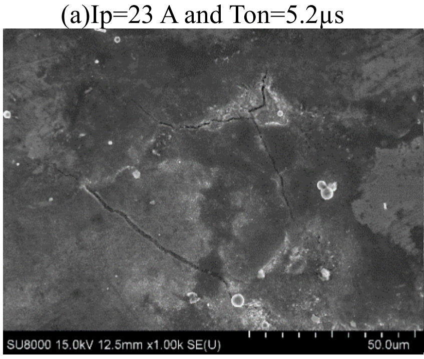

(c) Ip=23 A and Ton=15.2μs

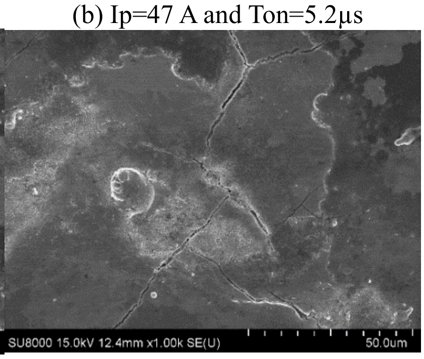

(d) Ip=47 A and Ton=15.2μs

Fig. 3 Surface microcracks on textured surfaces

The number of surface microcracks after electrical discharge machining (EDM) in groups (c) and (d) with a pulse width of 15.2 μs is significantly higher than that in groups (a) and (b) with a pulse width of 5.2 μs. As the pulse width increases, the duration of plasma impact on the workpiece surface within the discharge channel also increases, leading to higher machining energy and greater thermal stress around the workpiece surface. Consequently, the molten material formed by the high-temperature discharge is expelled by the surrounding thermal stress, resulting in the occurrence of microcracks.

(2) Surface spherical and molten flat bottomed structure. As shown in Figures 4, the electrical parameters are (a) peak discharge current of 35 A, pulse discharge width of 15.2 μ s, (b) peak discharge current of 60 A, pulse discharge width of 15.2 μ s. The special morphology of the surface microstructure after electrical discharge machining treatment was identified under a field emission scanning electron microscope.

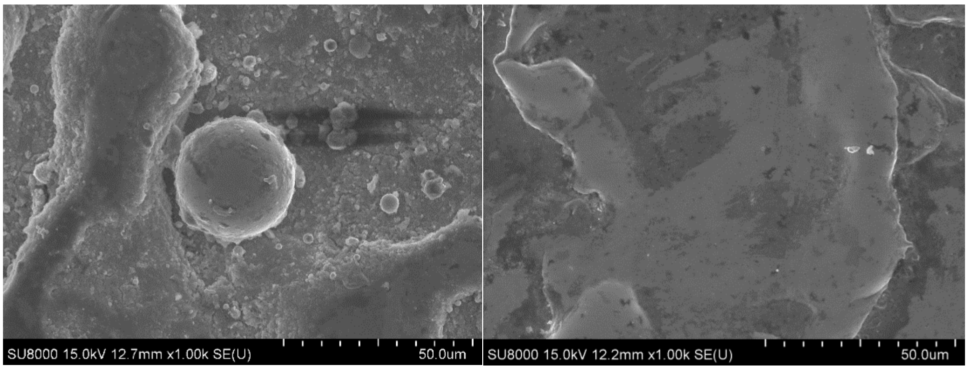

(a)Ip=35 A and Ton=15.2μs (b) Ip=60 A and Ton=15.2μs

Fig. 4 melting on textured surfaces

When the peak current is low at 35 A, the molten metal is thrown out by thermal stress, with a portion of the metal thrown into the working fluid and another portion of the molten metal thrown onto the surface of the workpiece to reattach and form spherical and granular shapes. With the increase of peak discharge current, the plasma density also increases. Within a single pulse time, the amount of plasma hitting the surface of the workpiece increases, thus accumulating extremely high energy in a short period of time, melting the original spherical structure and forming a clear flat bottomed pot shape, and the pores gradually disappear.

Experiments have shown that a pulse discharge width that is too high is prone to the formation of microcracks, while a peak discharge current that is too high is prone to the formation of molten structures. Whether it is microcracks or molten structures, using them in electromagnetic shielding of traction inverters is extremely disadvantageous. To avoid such phenomena, the pulse discharge width and peak discharge current value can be adjusted appropriately during later experimental processing to effectively reduce the adverse factors on the workpiece surface caused by roughening processing.

4. Research on the number of pits per unit length

4.1 The influence of pulse width on the number of pits per unit length

As shown in Figures 5, the special morphology of the hairy surface was observed under a 200x optical microscope with peak current Ip=60 A, pulse widths Ton=7.6 μ s (a), 9.6 μ s (b), 11.2 μ s (c), 13.6 μ s (d).

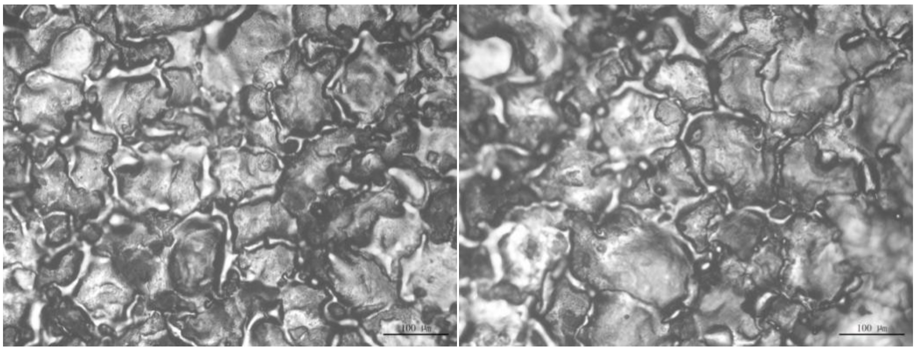

(a) Microscopic morphology at Ton=7.6μs (b) Microscopic morphology at Ton=9.6μs

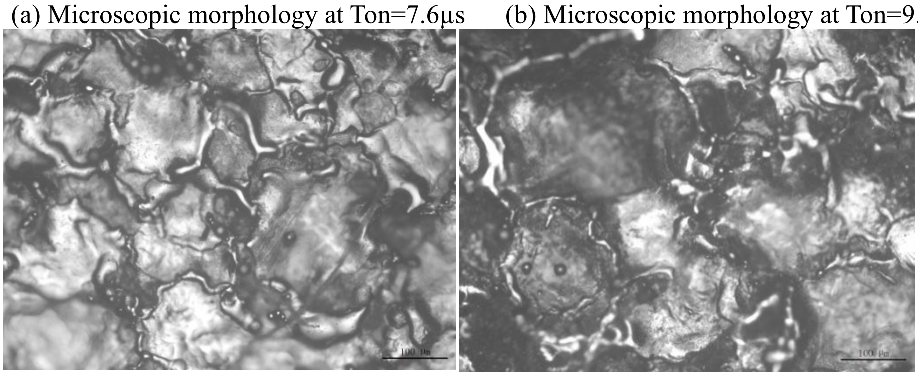

(c) Microscopic morphology at Ton=11.2μs (d) Microscopic morphology at Ton=13.6μs

Fig. 5 Micrograph of spark textured morphology of different pulse widths (Ip=60A)

When the peak current Ip is 60 A and the pulse width Ton is 7.6 μ s, the pulse width is extremely small, and the single processing time is short. The plasma in the discharge channel is difficult to impact the workpiece surface within the effective time, thereby releasing less energy [18,19], resulting in a smaller pit radius and a larger number of pits per unit length, When the pulse width Ton continues to increase from 7.6 μs to 13.6 μs, the effective time for plasma to impact the workpiece surface in the discharge channel increases due to the prolonged discharge time during a single pulse machining process. As a result, the axial and radial temperature gradients in the discharge channel decrease, indicating an increase in the average pit diameter and a decrease in the quantity of surface pits per unit length.

As shown in Figure 6, the variation curve of the quantity of surface pits per unit length with pulse width under different peak current conditions was measured using scanning electron microscopy after surface treatment.

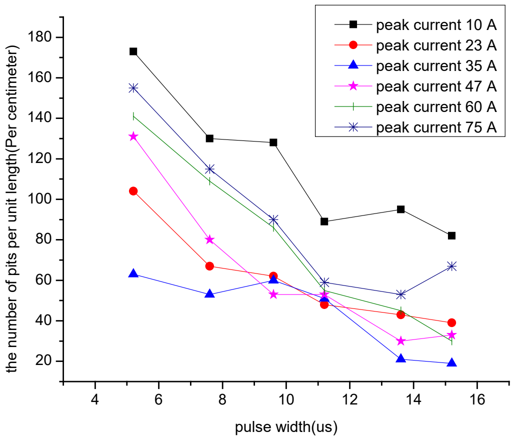

Fig. 6 Curve of the quantity of surface pits per unit length as a function of pulse width

From the curve graph, it can be seen that the quantity of surface pits per unit length under different peak current conditions generally decreases with the increase of pulse width, thus verifying the relationship between single pulse discharge energy and pulse discharge radius, and following the characteristics of the electric spark fuzz morphology under different pulse widths.

4.2 The influence of peak current on the quantity of surface pits per unit length

As shown in Figures 7, the special morphology of the hairy surface was observed under a 200x optical microscope with a pulse width Ton=7.6 μ s and peak currents Ip=10 A (a), 35 A (b), 47 A (c), and 60 A (d).

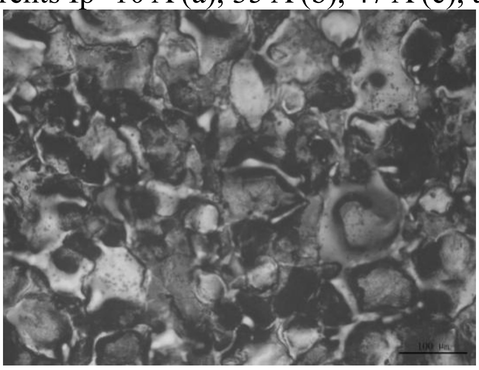

(a) Microscopic morphology at Ip=10 A

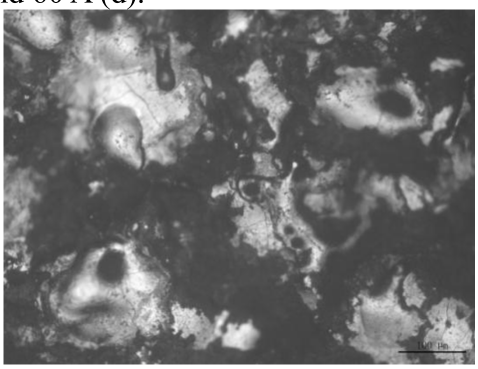

(b) Microscopic morphology at Ip=35 A

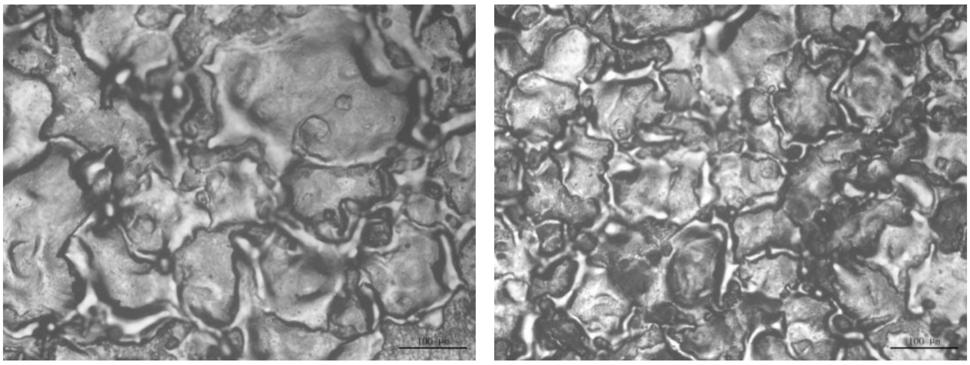

(c) Microscopic morphology at Ip=47 A (d) Microscopic morphology at Ip=60 A

Fig. 7 Micrograph of spark textured morphology of different peak current (Ton=7.6 μs)

When the pulse width Ton is 7.6 μs and the peak current Ip is 10A, the relationship $R = K_a I_P^{0.4} I_{on}^{0.5}$ between pulse energy and single pulse discharge radius shows that small peak currents result in lower spark discharge energy [20]. As a result, the diameter of the pits etched distributed on the workpiece surface formed by a single pulse machining is smaller, showing a phenomenon of a larger number of pits per unit length, When the peak discharge current is increased to 35 A, the plasma density and energy in the discharge channel increase with the gradual increment of peak discharge current, and the diameter of the etched pits begins to increase, that is, the quantity of surface pits per unit length decreases, When the peak discharge current continues to increase to 47 A, although the plasma density in the discharge channel further increases, the amount of molten metal particles and impurities formed by the surface electric spark discharge of the workpiece gradually increases. At this time, some of the energy in the electric spark discharge channel begins to be used to throw out the molten metal and residue eroded distributed on the workpiece surface due to discharge [21]. Therefore, the average pit diameter decreases instead, and the quantity of surface pits per unit length begins to show an increasing trend.

As shown in Figure 8, the variation curve of the quantity of surface pits per unit length with peak current under different pulse width conditions was measured using scanning electron microscopy after surface treatment.

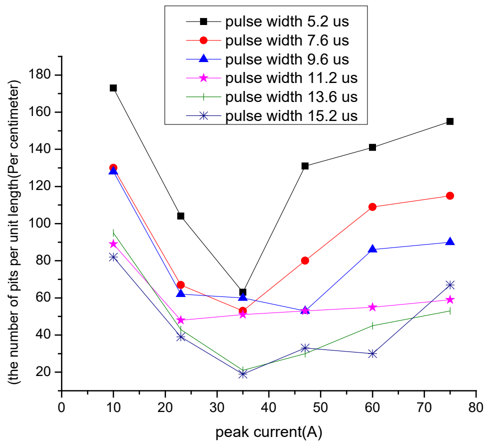

Fig. 8 Curve of the quantity of surface pits per unit length as a function of peak current

From the figure 8, it can be seen that the quantity of surface pits per unit length Pe manifests a general trend of decreasing first and then increasing as peak discharge current increases, which verifies the relationship between discharge energy and discharge radius, and follows the characteristics of electric spark fuzz morphology under different pulse discharge widths.

5. Modeling of roughened random rough surfaces relying on Monte Carlo method

The roughened surface of the traction inverter box presents a large number of stacked concave convex structures, which conform to the characteristic laws of Monte Carlo method [22,23]. The Monte Carlo simulation approach is utilized to simulate the surface characteristic morphology of electric spark roughening at relevant lengths. Assuming that the length of the two-dimensional stochastic rough surface to be created in the x and y directions is L_x and L_y, respectively, the number of equidistant scatter locations is M and N, and the distance between neighboring locations is Δx and Δy, respectively. Each point's height on the rough surface can be formulated as

$$f(x_m, y_n) = \frac{1}{L_x L_y} \sum_{m_k=-M/2+1}^{M/2} \sum_{n_k=-N/2+1}^{N/2} F(k_{m_k}, k_{n_k}) \exp[i(k_{m_k} x_m + k_{n_k} y_n)] \tag{1}$$

in the formula

$$F(k_{m_k}, k_{n_k}) = 2\pi \left[L_x L_y S(k_{m_k}, k_{n_k}) \right]^{1/2} \begin{cases} \dfrac{[N(0,1) + iN(0,1)]}{\sqrt{2}} & m_k \neq 0, M/2, \text{ and } n_k \neq 0, N/2 \\ N(0,1) & m_k = 0, M/2, \text{ or } n_k = 0, N/2 \end{cases} \tag{2}$$

In the formula $k_{m_k} = 2\pi m_k / L_x$, $k_{n_k} = 2\pi n_k / L_y$, power spectral density $S(k_x,k_y)$:

$$S(k_x,k_y)=\delta^2\frac{l_x l_y}{4\pi}\exp(-\frac{k_x^2 l_x^2+k_y^2 l_y^2}{4}) \tag{3}$$

δ —Root mean square (RMS) of surface elevation

l_x —Length related to the X direction

l_y —Length related to the Y direction

When $l_x = l_y$ =0.1 μm , δ =0.05, 0.1, 0.15 μm , the characteristic morphology of the hairy surface is obtained from Figure 9.

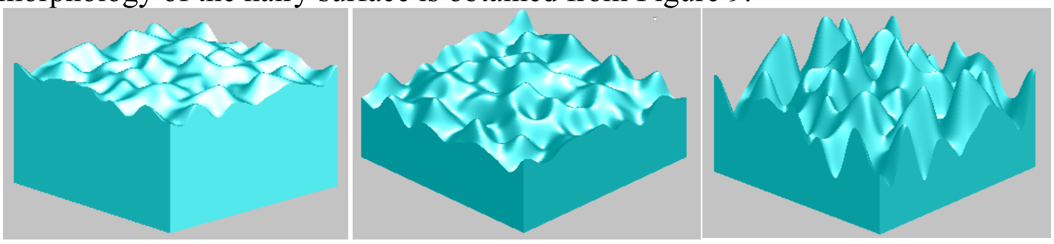

(a) δ =0.05 μm (b) δ =0.1 μm (c) δ =0.15 μm

Fig. 9 Simulation diagram of hairy surface at different δ ($L_x = L_y$ =0.1 μm)

When δ =0.1 μm , $l_x = l_y$ =0.05, 0.1, 0.5 μm , the characteristic morphology of the hairy surface is obtained from Figure 10.

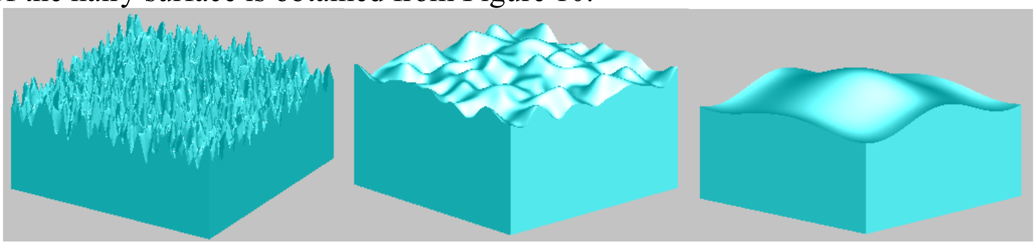

(a) $l_x = l_y$ =0.05 μm (d) (b) $l_x = l_y$ =0.1 μm (e) (c) $l_x = l_y$ =0.5 μm (f)

Fig. 10 Simulation diagram of hairy surface at different L (δ =0.1 μm)

6. Simulation results

6.1 The influence of root means square height on electromagnetic scattering from randomly rough surface

As shown in Figures 11, the distribution cloud map of electromagnetic field reflection waves on the roughened surface is shown in Figure 11, with a correlation length of 0.02μm and RMS 0.05μm (a), 0.15μm (b), 0.20μm (c), and 0.25μm (d), respectively.

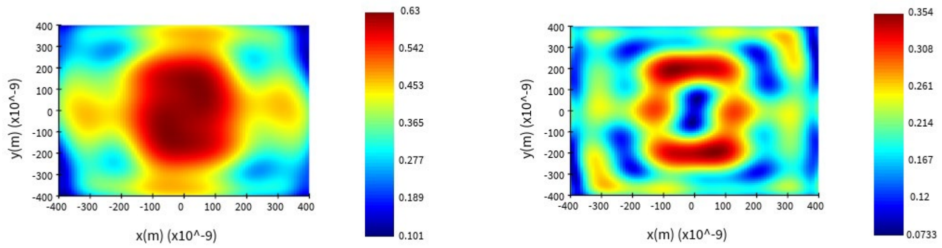

(a) Magnetic Field Distribution at δ =0.05 μm (b) Magnetic Field Distribution at δ =0.15 μm

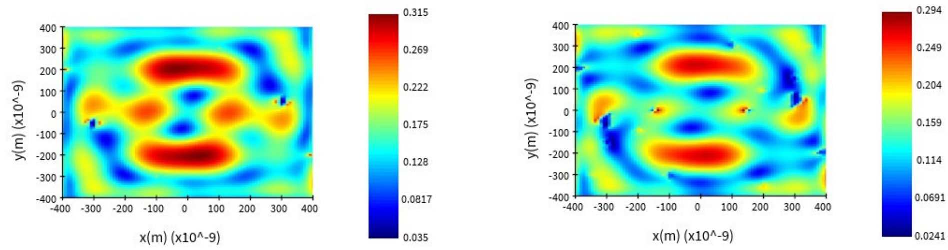

(c) Magnetic Field Distribution at δ =0.20 μm (d) Magnetic Field Distribution at δ =0.25 μm

Fig.11 Magnetic Field Distribution of Plane Wave In Textured Surface of Different δ

From the electromagnetic field intensity distribution map around the roughened surface detected by the reflection power monitor in the above figure, it can be seen that at the same correlation length, the electromagnetic field intensity of the reflected wave reveals a declining trend with the increase of RMS. Since the absorption rate=1 reflectivity transmittance, the transmittance is negligibly small. Therefore, the absorption rate is approximately equal to 100% minus the reflectivity. Therefore, the correlation length remains unchanged, and the absorption rate of the roughened surface is positively correlated with RMS increment.

The results presented in Figure 12 below, the variation curves of the average absorption rate are obtained under the simulation conditions of different root mean square values at different heights with corresponding lengths of 0.05μm, 0.15μm, 0.25μm, and 0.35 μm.

As shown in Figure 12, at the same correlation length, raising the RMS means that the average pit diameter of the roughened surface remains unchanged, while increasing the average pit depth increases the number of reflections of electromagnetic waves irradiated on its surface.

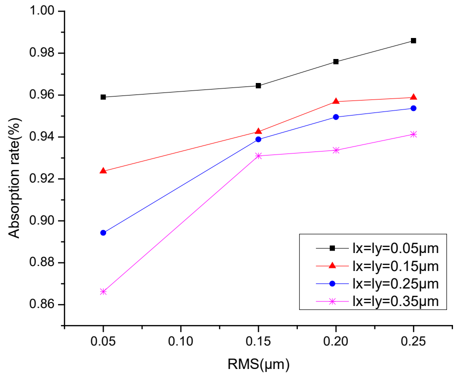

Fig. 12 Absorption Rate of Textured Surface Under Different δ

Most of the energy is sharply reduced after multiple reflections inside the material pit, resulting in a decrease in the energy reflected back to the outside world, that is, a decrease in reflectivity and an increase in absorption rate. Therefore, the simulated absorption rate (electromagnetic shielding) of the frosted surface exhibits an upward trend with the rise of the root mean square height.

6.2 The influence of correlation length on electromagnetic scattering from randomly rough surface

As shown in Figures 13, the distribution cloud map of electromagnetic field reflection waves on the roughened surface is illustrated in Figure 13, with a RMS height of 0.15μm and corresponding lengths of 0.05μm (a), 0.15μm (b), 0.25μm (c), and 0.35μm (d).

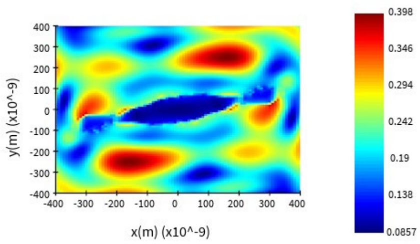

(a) Magnetic Field Distribution at L=0.05μm

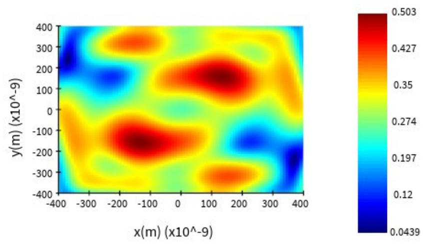

(b) Magnetic Field Distribution at L=0.15μm

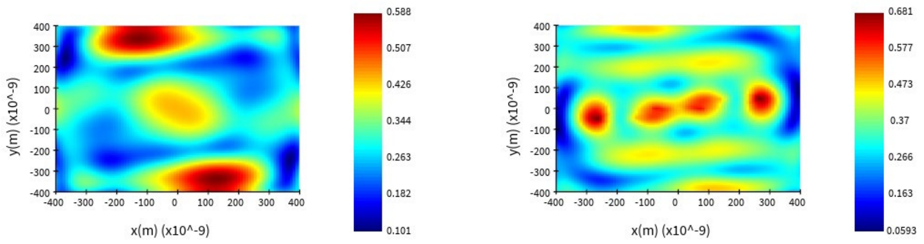

(c) Magnetic Field Distribution at L=0.25μm (d) Magnetic Field Distribution at L=0.35μm

Fig.13 Magnetic Field Distribution of Plane Wave In Textured Surface of Different l

According to the distribution of electromagnetic field intensity around the roughened surface detected by the reflection power monitor in the above figure, under the same root mean square condition at the same height, the electromagnetic field intensity of the reflected wave shows an overall increasing trend with the increase of correlation length. Therefore, while the RMS height remains unchanged, the absorption rate of the roughened surface decreases with the increase of the correlation length.

As shown in the corresponding Figure 14 below, the variation curves of the average absorption rate are obtained under different simulation conditions with RMS height of 0.05 μm, 0.15μm, 0.20μm, and 0.25μm, respectively.

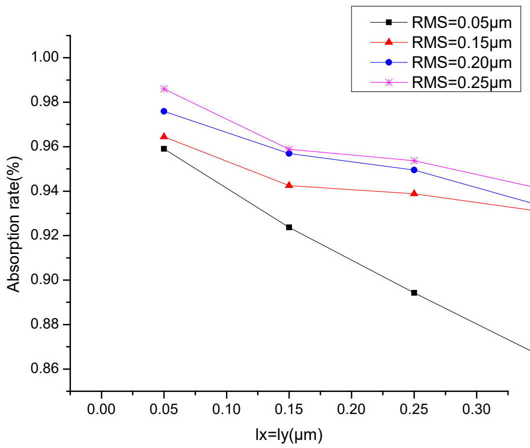

Fig. 14 Absorption Rate of Textured Surface Under Different l

As shown in Figure 14, under the same RMS height condition, increasing the relevant length means that the average pit depth of the roughened surface remains unchanged, the average pit diameter increases, that is, the quantity of surface pits per unit length decreases. However, the reflectivity of electromagnetic waves on the roughened surface is negatively proportional to the size of the average pit diameter, that is, the reflectivity declines significantly with the gradual increment of the average pit diameter and exhibits an upward trend with the growth of the quantity of surface pits per unit length. This is mainly because increasing the average pit diameter reduces the average quantity of surface pits per unit length area, resulting in a greatly increased probability of electromagnetic waves being reflected on its surface. Therefore, the absorption rate decreases accordingly.

6.3 Effect of root mean square height to relevant length ratio on electromagnetic scattering from randomly rough surfaces

From the above simulation results, it can be seen that there is a certain regularity between the electromagnetic shielding characteristics of the roughened surface and the RMS height and the correlation length. The RMS/l characterizes the ratio of the depth to the diameter of the micro-pits. In order to further study the influence of the ratio of the depth to the diameter of the micro-pits on the electromagnetic shielding of the roughened surface, it is necessary to comprehensively analyze the two factors of the RMS height and the related length, and further study the variation of electromagnetic shielding with the ratio of the RMS height to the related length.

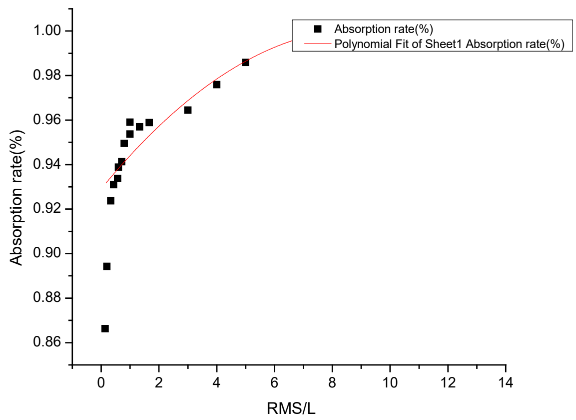

Fig.15 Absorption Rate of Textured Surface Under Different RMS/l

From Figure 15, it can be seen that the absorption rate of the roughened surface generally shows an increasing trend with the ratio of the root mean square of height to the relevant length, which means that the depth to diameter ratio of the pits on the roughened surface of the material increases. The frequency of electromagnetic waves reflected on its roughened characteristic surface increases, that is, the probability of electromagnetic waves being repeatedly absorbed increases. The ratio increases from 0.2 to 5.8, the absorption rate increases from 86.6% to 98.4%, and the electromagnetic shielding effect improves by 13.6%.

7. Conclusion

This paper adopts the single factor control variable method for experiments, and conducts a six level orthogonal experiment with pulse width and peak current as two factors, the research results indicate that Excessive pulse width can indicate the formation of microcracks, while excessive peak current can lead to the formation of molten structures. The quantity of surface pits per unit length generally decreases with the increase of pulse width, and a trend of first decrease followed by increase is exhibited as peak current grows continuously. Through simulation analysis, it is found that the absorption rate of the roughened surface decreases with the increase of relevant length, and increases with the increase of the quantity of surface pits per unit length. That is, the absorption rate of the roughened surface decreases with increasing pulse width, it exhibits a bimodal trend of initial decrease and subsequent increase with the growth of peak current. The surface absorption rate of the roughened surface shows an overall increasing trend with the ratio of the depth to the diameter of the micro-pits. The ratio of the depth to the diameter of the micro-pits increases from 0.2 to 5.8, the absorption rate increases from 86.6% to 98.4%, and the electromagnetic shielding effect improves by 13.6%. This provides a reference and direction for its application in the research of electromagnetic shielding of traction converters for high-speed trains.

Acknowledgement

Fund Project: This work was supported by the 2023 Guangxi University Young and Middle aged Teachers Research Basic Ability Enhancement Project "Research on Electromagnetic Shielding Technology of Traction Converter Box Based on Electric Spark Roughening Process" (2023KY1439).

REFERENCES

[1] *Wu E T, Qiu M B, Yao Z X, et al*. Experimental Study on Step-by-Step Electrical Discharge Machining of Square Blind Holes in TC4 Titanium Alloy. International Journal of Precision Engineering and Manufacturing, 2024, 25(5):933-945.

[2] *Padhy P K, Sarmah P, Patowari P K* .Machining of Microchannel Using Wire Electrical Discharge Machining and Its Parametric Study. Lecture Notes in Mechanical Engineering, 2025:349-356.

[3] *Sun X W, Yang Y, Li Y Q, et al*. Study on the microstructure and properties of Zr-4 alloy after electrical discharge machining. Tool Technology, 2025, 59 (02): 23-29.

[4] *Sedat G, Yilmaz M, Gkkaya H, et al.* Determination of the Optimum Conditions for Machining NiTi Shape Memory Alloys by Electrical Discharge Machining. Journal of The Institution of Engineers (India): Series C, 2024, 105(5):1035-1046.

[5] *Iqbal A, Hassan T, Naqvi S M, et al.* Menes for multispectral electromagnetic shielding. Nature Reviews Electrical Engineering, 2024, 1(3):180-198.

[6] *Yang D Y, Zhu B Q, Chen Y, et al*. Research on Electromagnetic Interference Analysis and Suppression Methods of High speed EMU Traction System. Locomotive Electric Transmission, 2022, (06):87-94.

[7] *Zhang S B, Wang F Q.* Design of Composite Traction Converter Box and Evaluation of Electromagnetic Pulse Protection Performance. Rail Transit Materials, 2022, 1 (01):47-52.
[8] *Devika S J, Kallyani A, Damodarakurup S, et al.* Conducting Carbon Black and Fe3O4-Reinforced Polydimethylsiloxane Composites for Electromagnetic Interference Shielding. Journal of Electronic Materials, 2025, 54(12):11696-11713.
[9] *Jiang D S, Liu Q Y, Chen Z H, et al*. Research on Discharge Energy Distribution in Micro EDM. Journal of Qingdao University of Technology, 2024, 45 (04): 139-145.
[10] *Liu Y X, Cui W M, Yang B, et al.* The influence of different electrical discharge machining parameters on the microstructure and impact properties of TA15. Information Recording Materials, 2025, 26 (03): 32-35.
[11] *Sun Y, Dong J Y, Tang B J, et al.* Surface Quality and Forming Accuracy of Single Crystal Silicon Microstructure by Electric Discharge Machining. Journal of Northeastern University (Natural Science Edition), 2025, 46 (02): 96-103.
[12] *Wei H, Wang F, Zhou J,et al*. Study of hole sucking on debris evacuation and processing efficiency in EDM of integral shrouded blisks. International Journal of Advanced Manufacturing Technology, 2025, 139(1).
[13] *Lauwers D, Sambou E T, Herrig T, et al.* Numerical analysis of the impact of the ECM inlet geometry on the electrolyte flow and its interaction with a thin-walled workpiece. Procedia CIRP, 2025, 137(000):259-264.
[14] *Bhat S S, Gummadi A K, Latha A, et al*. Electric Discharge Machining of AA7075/SICP/B4CP Hybrid Composites Machined with AL2O3 Mixed used Engine Oil Dielectric Fluid. Current Materials Science, 2025, 18(5):18.
[15] *Hiroshi I, Naonari S, Yasuhiro S T* .Facile synthesis of electrocatalytically active Cu/graphite using the negative electrode of spent Li-ion batteries. Green chemistry, 2024, 26(4):2190-2197.
[16] *Liang H N, Liu Z Q, Chen D L, et al.* Analysis of Surface Texture EDM Process Parameters for Embossing Molds. Metal Heat Treatment, 2022, 47 (03): 20-27.
[17] *Dubey V, Sharma A K, Singh B* .Optimization of machining parameters in chromium-additive mixed electrical discharge machining of the AA7075/5%B4C composite:. Proceedings of the Institution of Mechanical Engineers, Part E: Journal of Process Mechanical Engineering, 2022, 236(1):104-113.
[18] *Sharma P, Kishore K, Singh V, et al.* Surface Morphology Analysis of Inconel 625 through Multi-walled Carbon Nanotubes-Based Electric Discharge Machining. Journal of Materials Engineering and Performance, 2025, 34(11):9813-9824.
[19] *Yang X D, Li Q.* Progress in Observation and Simulation Research of Electric Discharge Machining Process. Electric Machining and Mold, 2025, (01): 1-14.
[20] *Liao Y, Dong S J, Li J Y, et al.* Research status of the influence of electrical discharge deposition process parameters on coating quality. Journal of Wuhan University of Light Industry, 2023, 42 (02): 89-96.
[21] *Liu Q Y, Sha R, Wang Y Q, et al*. Research on the machining characteristics of SiCp/Al composite nano mixed powder electric discharge electrolytic composite. Electrical Machining and Mold, 2025, (S1):66-74.
[22] *Zhixu D, Shu Y, Pengtao B, et al*., Modeling and characteristic analysis of reflection polarization on coating surface based on Monte Carlo method. Optical engineering, 2024, 63(10):15.
[23] *Chai X Y, Hu H, Hu X X, et al.* Research on Surface Scattering and Imaging Characteristics of Rough Targets in Terahertz Low Frequency Band. Advances in Laser and Optoelectronics, 2024, 61 (10): 166-174.